VOLUME 156 • NUMBER 2 • FEBRUARY 2009

ELSEVIER

Combustion and Flame

THE JOURNAL OF THE COMBUSTION INSTITUTE

Available online at www.sciencedirect.com

ScienceDirect

Enhanced reactivity of nano-B/Al/CuO MIC's

K. Sullivan, G. Young, M.R. Zachariah *

Department of Mechanical Engineering and Department of Chemistry and Biochemistry, University of Maryland – College Park, College Park, MD 20740, USA

A B S T R A C T

Aluminum is traditionally used as the primary fuel in nanocomposite energetic systems due to its abundance and high energy release. However, thermodynamically boron releases more energy on both a mass and volumetric basis. Kinetic limitations can explain why boron rarely achieves its full potential in practical combustion applications, and thus has not replaced aluminum as the primary fuel in energetic systems. In particular, the existence of the naturally formed boron oxide (B_2O_3) shell is believed to play a major role in retarding the reactivity by acting as a liquid barrier if it cannot be efficiently removed. In this paper we demonstrate from constant-volume combustion experiments that nanoboron can be used to enhance the reactivity of nanoaluminum-based Metastable Intermolecular Composites (MICs) when the boron is <50 mol% of the fuel. It was also observed that an enhancement was not achieved when micronboron (700 nm) was used. Thermodynamic calculations showed that the aluminum reaction with CuO was sufficient to raise the temperature above ~2350 K in those mixtures which showed an enhancement. This is above both the boiling point of B_2O_3 (2338 K) and the melting point of boron (2350 K). A heat transfer model investigates the heating time of boron for temperatures >2350 K (the region where the enhancement is achieved), and includes three heating times; sensible heating, evaporation of the B_2O_3 oxide shell, and the melting of pure boron. The model predicts the removal of the B_2O_3 oxide shell is fast for both the nano- and micronboron, and thus its removal alone cannot explain why nanoboron leads to enhancement while micronboron does not. The major difference in heating times between the nano- and micronboron is the melting time of the boron, with the micronboron taking a significantly longer time to melt than nanoboron. Since the oxide shell removal time is fast for both the nano- and micronboron, and since the enhancement is only achieved when the primary reaction (Al/CuO) can raise the temperature above 2350 K, we conclude that the melting of boron is also necessary for fast reaction in such formulations. Nanoboron can very quickly be heated relative to micronboron, and on a timescale consistent with the timescale of the Al/CuO reaction, thus allowing it to participate more efficiently in the combustion. The results indicate that sufficiently small boron can enhance the reactivity of a nanoaluminum-based MIC when added as the minor component (<50% by mole) of the fuel.

© 2008 The Combustion Institute. Published by Elsevier Inc. All rights reserved.

1. Introduction

Energetic materials consisting of a metal as a fuel and a metal oxide as an oxidizer with particle sizes in the nanometer range are termed Metastable Intermolecular Composites (MICs) and give rise to thermite reactions upon ignition. Such materials have received considerable attention due to their high energy densities and reaction temperatures, and their potential use in explosives, pyrotechnics, and propellants is currently being investigated. Perhaps the single most attractive feature of a MIC is that the reactivity can be tuned through easily-adjustable parameters (i.e. particle size, stoichiometry, etc.) making them prime candidates for a wide range of end-user applications, such as initiators for explosives or enhancers for propellants. Traditionally, aluminum has been used as the fuel

in thermites due to a combination of its high energy release and its abundance. However, thermodynamically boron is an attractive alternative since it has higher heating values on both a mass and volumetric basis. Table 1 shows the heating values of some metals which could be potential candidates. Other than beryllium, which is not practical due to its toxicity, boron shows higher heating values than all of the other metals.

When exposed to air, aluminum and boron form an oxide shell around the elemental core of fuel. The shell is typically only a few nanometers thick and, on a supermicron level, is an insignificant amount of the particle mass. However, as the particle size transitions into the nanometer regime, the shell becomes a larger portion of the total mass and can play a critical role in the combustion process. Though the heating values clearly suggest that boron should outperform aluminum, the burning mechanisms of these two materials are speculated to be quite different when one takes into consideration the core–shell structure.

---

* Corresponding author.
E-mail address: mrz@umd.edu (M.R. Zachariah).

Table 1
Heating values per mass and volume for various metals.

Metal	ΔH per unit mass (kcal/g)	ΔH per unit volume (kcal/cc)
Boron	−14.12	−33.19
Beryllium	−15.88	−29.38
Aluminum	−7.41	−20.01
Titanium	−4.71	−21.20
Vanadium	−3.64	−21.69
Magnesium	−5.91	−10.28
Nickel	−0.98	−8.72

Different theories have been suggested to explain the burning of an aluminum particle with its elemental core and oxide shell. Initially, Glassman [1,2] proposed that metal combustion is similar to droplet combustion, and therefore a D^2 model could be employed to describe the burn time. He further suggested that the ignition and combustion processes would be governed by the melting and boiling points of the metal and metal oxide. Price [3] suggested two possible mechanisms for the breakdown of the aluminum oxide shell and ignition of aluminum particles. The first mechanism involves the very different melting temperature of aluminum oxide (2327 K) and pure aluminum (930 K). As a result, upon particle heating, the elemental core melts and the molten aluminum expands. This induces thermal stresses in the oxide shell, leading to cracks that expose molten aluminum to the oxidizing species. The other possibility is that the oxide layer undergoes melting itself, which would require much higher temperatures for ignition.

More recently, Trunov et al. [4] studied the effects of phase transformations in the oxide shell upon heating. They used thermogravimetric analysis and X-ray diffraction to study the oxidation of aluminum particles with various sizes and morphologies, and found that aluminum combustion can be explained by a four-stage process. During the first stage, the thickness of the initial amorphous oxide shell increases until it reaches a critical value of about 5 nm. The next stage involves the transformation of the oxide layer into denser γ-Al_2O_3, exposing some of the core aluminum. In the third stage, the γ-Al_2O_3 layer grows and partially transforms into θ-Al_2O_3 and δ-Al_2O_3. Finally, stage four involves the transformation of the shell into stable α-Al_2O_3. In recent work by our group on nanoaluminum, Rai et al. [5] found that aluminum melting was necessary for fast reaction, and was due to the counter diffusion of aluminum metal out rather than oxidizer to the core. This results in the formation under some conditions of a hollow alumina product. Olsen and Beckstead [6] also showed the formation of a hollow product in combustion studies of micron-sized particles.

In boron, a different observation is made during particle heating. Similar to aluminum, a boron particle has an oxide shell (B_2O_3) which surrounds the elemental boron core. The oxide layer, however, melts at a much lower temperature (722 K) than the core (2375 K), rendering a different burning scenario than aluminum. Upon heating, the oxide shell will melt before the solid core, thus leading to a diffusion-controlled process through the molten shell. The pioneering work of Macek and Semple [7] suggested that boron combustion always happens in a two-step process, separated by a dark period. The first step involves the removal of the oxide layer, while the second step involves the burning of a bare boron particle in air. Ulas et al. [8] also support that the combustion of boron particles is defined by a two-stage process. Again, the first stage of boron combustion was considered as the removal of the oxide layer. This process is a slow, kinetic and/or diffusion controlled process, which constitutes a significant portion of the overall burning time of the particle. After removal of the oxide

layer, the second stage begins with the combustion of the pure boron.

Contradicting theories about the treatment of diffusion through the molten B_2O_3 layer have been proposed, with Glassman [9] suggesting that elemental boron dissolves into the molten B_2O_3 layer and diffuses outward to the $B_2O_{3(L)}$/gas interface, while King [10–13] suggested that O_2 dissolves into the molten layer and inwards to the $B/B_2O_{3(L)}$ interface. This argument has been more recently addressed in a review article by Yeh and Kuo [14], where they report that the diffusion of boron into the molten $B_2O_{3(L)}$ dominates the diffusion process. They also report the formation of a polymeric vitreous $(BO)_n$ complex in the reaction between dissolved boron and molten B_2O_3. These results were used to develop a reaction mechanism for boron combustion.

Aluminum and boron differ in their combustion mechanisms primarily due to the inherent properties of the pure material and their oxides. Based upon Glassman's Criterion [15], aluminum will combust in a vapor phase in an oxygen environment since its oxide's volatilization temperature is higher than the boiling point of pure aluminum. On the other hand, boron will not combust in the vapor phase since the boiling point of pure boron is significantly higher than the volatilization temperature of its oxide. In fact, since boron oxide melts at a much lower temperature than pure boron, it covers the particle and creates a substantial diffusive barrier between the oxidizer and pure fuel.

Despite the great potential of boron as a fuel, it has rarely achieved its potential in systems that require fast and complete combustion. Ulas et al. [8] suggest there are two major reasons for this; (1) the ignition of boron particles is significantly delayed due to the presence of an oxide layer on the particle surface, and (2) the energy release is during the combustion process of boron particles in hydrogen containing gases is significantly lowered due to the formation of HBO_2. Yetter [16] adds to these issues the idea of an energy trap. Hydrogen containing species can accelerate the gas-phase combustion process. Unfortunately they promote the formation of HBO_2, which is thermodynamically favored over gaseous B_2O_3 as the temperature is lowered, which can result in the boron being "trapped" as HBO_2 and therefore not releasing all of its available energy. The energy trap arises from the fact that from an energetic standpoint, the best product of boron combustion is liquid boron oxide. Even in non-hydrogen containing environments, the quickest way to remove the oxide layer and combust the pure boron material is at temperatures above the B_2O_3 boiling point of 2338 K. However, combustion at these temperatures would result in the formation of $B_2O_3(g)$ whose heat of formation is approximately one third of the liquid form. Furthermore, in early studies Macek [17] showed that boron particles had burn times up to four times longer than similar sized aluminum in similar environments.

Most recently, an effort has been made to address the issue of oxide layer removal. Difluoroamino-based oxidizers have been developed, and have rejuvenated the hopes for boron combustion. With fluorine as an oxidizing agent, an increase in gas-phase combustion products can be realized; a desired effect for energetic materials. Ulas et al. [8] combusted single boron particles in fluorine-containing environments by injecting particles into the post flame region of a multi-diffusion flat-flame burner. Their results show the disappearance of the apparent "two-step" combustion process in the presence of fluorine, along with decreased burning times. This is a major result for boron combustion since the removal of the oxide layer adds significantly to the overall burning time, and if the oxide layer can be removed more efficiently, then boron might be able to be practically used in energetic formulations.

The primary work on boron particle burning has been studied with particle sizes in the micron range, and few works have investigated the use of nanoboron in composite systems. In separate works, Hunt and Pantoya [18] and Park et al. [19] have shown

decreasing activation energies with decreasing particle sizes, leading to increased reactivity. A lower activation energy should also imply a lower ignition temperature, and this was indeed corroborated by various authors such as Parr [20] and Bazyn [21]. When nanoaluminum is used in place of its micron-sized counterpart in composite systems, an increase of 1000 in the reactivity has been reported [22], therefore, we wanted to investigate the performance of nanoboron in such systems. It will be demonstrated from constant-volume combustion experiments that nanoboron, while very unreactive itself, can be used to enhance the reactivity of nanoaluminum-based MICs. We develop a heat transfer model for boron particles surrounded by an aluminum thermite reaction, and propose that the aluminum reaction augments the burning of the boron by providing a high-temperature environment for fast ignition and combustion of the boron.

2. Experimental

2.1. Sample preparation

For this work, stoichiometric samples (MICs) were prepared with the fuel being composites of boron and aluminum, and the oxidizer always being copper oxide. We will refer to the samples in terms of the molar percentage of boron in the fuel. For example, a 30% B sample means that 30% of the fuel atoms are boron, 70% are aluminum, and the corresponding amount of copper oxide is added to make the overall mixture stoichiometric assuming complete conversion to Al_2O_3 and B_2O_3. The aluminum used was obtained from the Argonide Corporation, and designated as "50 nm ALEX" by the supplier. ALEX is a nano-sized aluminum formed from the electroexplosion of an aluminum wire [23]. The nanoboron utilized in this study was termed SB99 and was obtained from the SB Boron Corporation. The average primary particle diameter is given to be 62 nm [24]. A second boron sample designated as SB95 was also obtained from the SB Boron Corporation. SB95 is an amorphous boron powder with particles sizes ranging up to 700 nm, as measured by a Fisher Sub-Sieve Sizer (FSSS). The oxidizer was copper (II) oxide nanopowder purchased from Sigma Aldrich, and had an average primary particle diameter specified by the supplier to be <50 nm. Thermogravimetric Analysis (TGA) was performed (using a 50/50 Ar/O_2 environment and a heating rate of 5 K/min up to 1200 °C) on both the aluminum and SB99 boron samples to determine the amount of elemental metal (active content or activity) in the particles. TGA showed the aluminum to be 82% active, while the SB99 boron was found to be 72% active by mass. The SB95 active content was 96%, specified by the supplier. A summary of the materials used is given below in Table 2.

MICs were prepared by first weighing out the fuel and oxidizer and adding the contents to a ceramic crucible. Approximately 10 mL of hexane was then added, and the mixture was sonicated for 20 min to ensure intimate mixing of the fuel and oxidizer particles. The hexane was then allowed to dry and then the samples were placed in a furnace at 100 °C for a few minutes to drive off any remaining hexane. The powders were then very gently broken apart with a spatula until the consistency for each sample was that of a loose powder.

2.2. Measurement of reactivity

The reactivity of a MIC has been shown to be closely correlated to two properties; the flame propagation velocity in open-channel burn tests, and the constant-volume pressurization rate. Both are relative measurements which are used by several authors to determine the reactivity [25–28]. In this work, we use

Table 2
A summary of nanopowders used in this work, including average primary particle diameter and active amount by mass.

Fuel	Source	Avg primary particle diameter	Measured by	Active content	Measured by
Al	ALEX	50 nm	TEM	82%	TGA
B	SB-99	62 nm	Reference [23]	72%	TGA
B	SB-95	700 nm	FSSS	96%	Supplier
Oxidizer					
CuO	Sigma–Aldrich	<50 nm	Sigma–Aldrich		

the pressurization rate inside a small combustion cell as a measurement of the reactivity. A fixed mass (25 mg) of the sample powder was placed inside a constant-volume (~13 mL) pressure cell. A schematic and more details of the pressure cell can be found in a previous publication [29]. A nichrome wire coupled to a voltage supply was placed in contact with the top of the powder, and served as an ignition source through resistive heating of the wire. A piezoelectric pressure sensor was used in series with an in-line charge amplifier and a signal conditioner, and the resultant voltage trace was captured on a digital oscilloscope upon ignition of the sample. The pressurization rate was calculated by converting the voltage rise to pressure (1 mV = 0.237 psi), and dividing by the rise time in microseconds. This was repeated three times for each sample, and the average pressurization rate (psi/us) was recorded.

Pressure signals of various samples are shown in Fig. 1 as an example of the kind of typical data obtained for the combustion tests. We show two "slow" reactions (90% and 70% B) along with two "fast" reactions (50% and 30% B), and the reader should note that the time scale is very different. Decreasing the time scale causes a noisier signal, but is necessary in order to capture the first peak with finer time resolution. Another thing to point out in the signal is shock waves "ringing" off the walls, seen in the data as oscillatory behavior of the signal after the first peak. In all of these pressure traces, the first oscillation can be seen around 120 us after the first major peak (this is most obvious in the 70% B trace). This corresponds to the approximate time it takes for a pressure wave to reflect off the wall directly opposite the sensor. In the two "fast" pressure traces, there are some new peaks (i.e. around 50 μs). These could be caused by some secondary burning within the system, and we should not rule this out as a possibility. However, it may also be simply an artifact of the geometry and/or ejection of the powder after the pressure wave reflects off other walls of the cell or the sample holder.

In order to extract the rise time in a consistent way, we always take the first major peak in the system (usually the maximum voltage) and apply a linear fit. We report the average of three tests, and the uncertainty is calculated from the standard deviation of the data.

3. Results and discussion

Shown in Fig. 2 is the pressurization rate as a function of % B in an Al/B/CuO mixture for both 62 nm and 700 nm boron, along with data from a MIC of Al/CuO for comparison. It can be seen that, when compared to pure Al/CuO, an enhancement in reactivity is achieved for the cases where nanoboron is added as the minor component of the fuel (<50% by mol). It is also clear that a MIC comprised of boron as the primary fuel is quite ineffective and considerably underperforms an aluminum-based MIC. It can also be seen that, not only is 700 nm boron less reactive than its nano-counterpart, but there is no enhancement effect when added to nanoaluminum in any amount.

Given that the data suggests that an enhancement in MIC burning occurs only when boron is the minor component, it is reason-
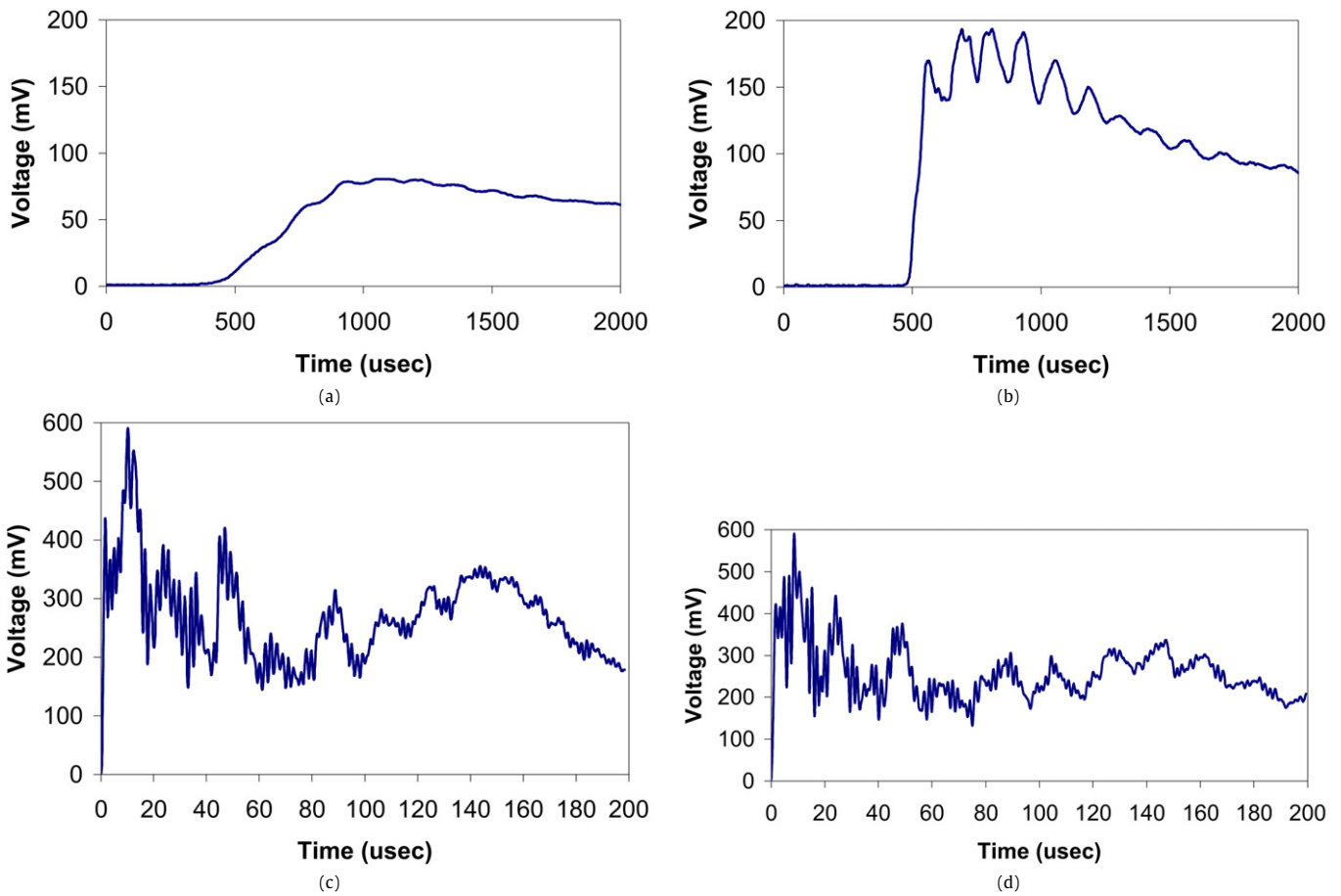
Fig. 1. Pressure traces for (a) 90% (slowest), (b) 70%, (c) 50%, and (d) 30% (fastest) B.
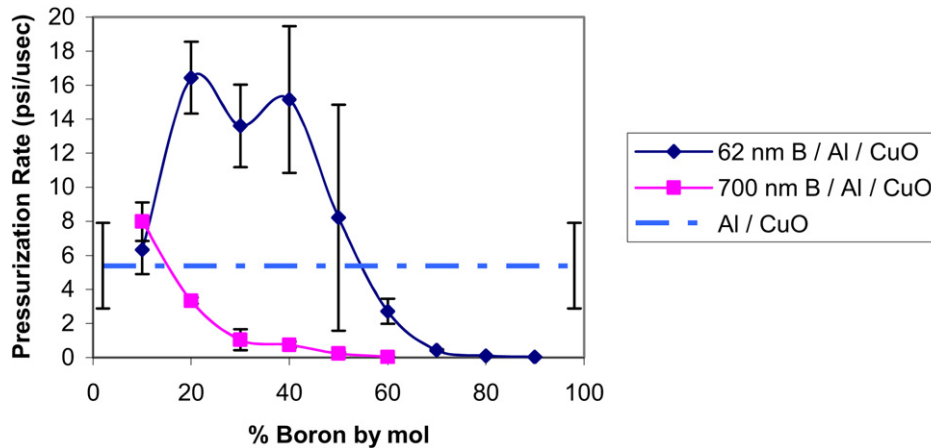

Fig. 2. Experimental pressurization rate as a function of % boron in an Al/B/CuO MIC for both nano- and micron-sized boron. The horizontal line is Al/CuO data, included for comparison. Error bars represent the standard deviation of the experimental data.

able to speculate that the primary reaction (Al/CuO) is allowing for efficient ignition and combustion of the boron. The enhancement begins at <50% B by mol, and so we sought an explanation as to why this point was important. In order to examine this, an appropriate thermodynamic calculation is to look at the adiabatic flame temperature assuming that the aluminum reacts with the copper oxide, while the boron is acting as an inert material. The CHEETAH code (using the JCZS product library [30] as recommended by Sanders et al. [28]) was used to calculate the adiabatic flame temperature for the various mixtures (assuming the boron to be inert) and the results are shown in Fig. 3. From Fig. 3 we see that the

mixtures with <50% B can reach temperatures higher than 2350 K, which is above the boiling point of B_2O_3 (2338 K) and the melting point of B (2350 K). Given that the experiment also showed an enhancement in this regime, it suggests that the primary reaction (Al/CuO) provides the energy necessary to remove the oxide shell and/or melt the boron, and thus enable it to participate in the combustion and enhance the reactivity. The removal of the oxide shell was discussed earlier as being necessary, while the melting of a nanoparticle can increase its reactivity significantly by allowing the fuel to become more mobile, as was seen by Rai et al. [5] for nanoaluminum.
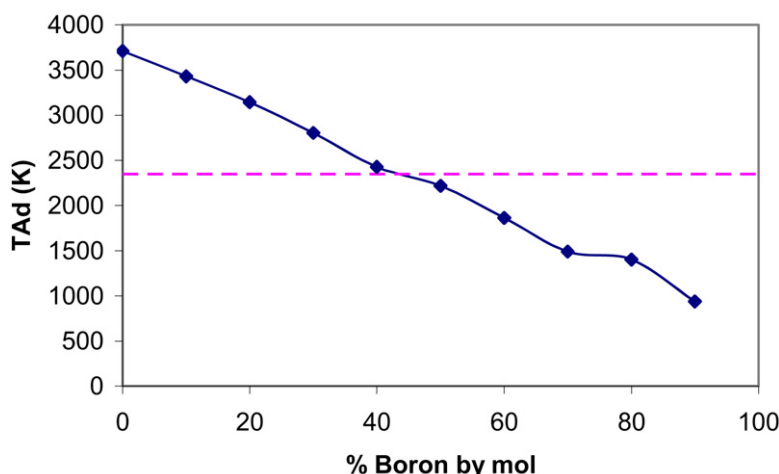
Fig. 3. Adiabatic flame temperature calculations for Al/B/CuO mixture. B is considered inert in these calculations. Boiling temperature of B_2O_3 = 2338 K.
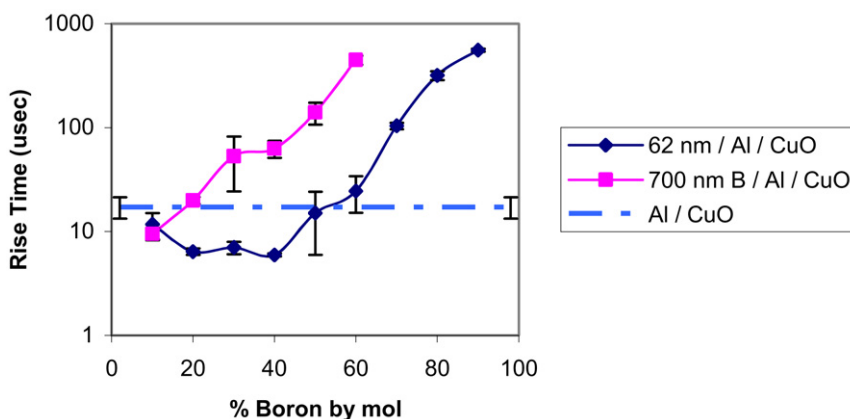

Fig. 4. Experimental rise times as a function of % B in an Al/B/CuO MIC for both nano- and micron-sized boron. The horizontal line is Al/CuO data, included for comparison. Error bars represent the standard deviation of the experimental data.

Shown in Fig. 4 are the experimentally measured rise times, and included are the 62 nm and 700 nm boron along with the 17 µs rise time for the Al/CuO reaction. Clearly, addition of the smaller boron decreases the rise time below that of Al/CuO when added as the minor component, while the larger boron only slows the reaction down. The data indicates that the 62 nm boron is participating in the combustion, and so an appropriate calculation should compare the timescale of the Al/CuO reaction (17 us) to the timescale of heating a boron particle up to the surrounding temperature so that it can combust. A heat transfer model is developed to investigate these time scales when the surrounding temperature is above 2350 K, the point where the experimental enhancement is observed.

3.1. Phenomenological heat transfer model

Here we develop a simple heat transfer model for a boron particle in a high temperature ($>$2350 K) environment. Several assumptions are made to simplify the problem:

(1) The Al and CuO particles are evenly distributed about single boron particles.
(2) The B_2O_3 shell thickness is 3.1 nm and 4.5 nm for the 62 nm and 700 nm particles, respectively. This is calculated by using the particle size, active content by mass, and bulk densities of B and B_2O_3 (2.34 g/cm^3 and 2.46 g/cm^3, respectively).
(3) The convective term only considers energy transferred through collisions with gas molecules.

(4) Interparticle radiation was found to make little difference to the model results, and thus was not included.

With the above assumptions in place, heat is convectively transferred to the particle by the gaseous species present during the Al/CuO reaction. The convection term can be written as the product of the heat transfer coefficient, h, the particle surface area, A, and the temperature difference between the surrounding environment and the particle.

$$\dot{q}_{conv} = hA(T - T_P). \tag{1}$$

The heat transfer coefficient for a solid sphere in a gaseous environment can be written in terms of the particle Nusselt number, Nu, the thermal conductivity of the gas, k_G, and the particle diameter, d_P, as

$$h = \frac{Nu\,k_G}{d_P}. \tag{2}$$

For particles with diameters much greater than the mean free path of the gas, the Nusselt number approaches a constant value of 2. However, the particle sizes in this work are comparable to the mean free path, and thus are in a transitional regime between continuum and free-molecular heat transfer. In this regime, the Nusselt number is a function of the particle Knudsen number [31]. The adiabatic flame temperature and the experimental peak to peak pressure rise, shown in Fig. 5, are used to estimate the mean free path, and thus the particle Knudsen numbers. The corresponding Nusselt numbers are then obtained from Fig. 4 in
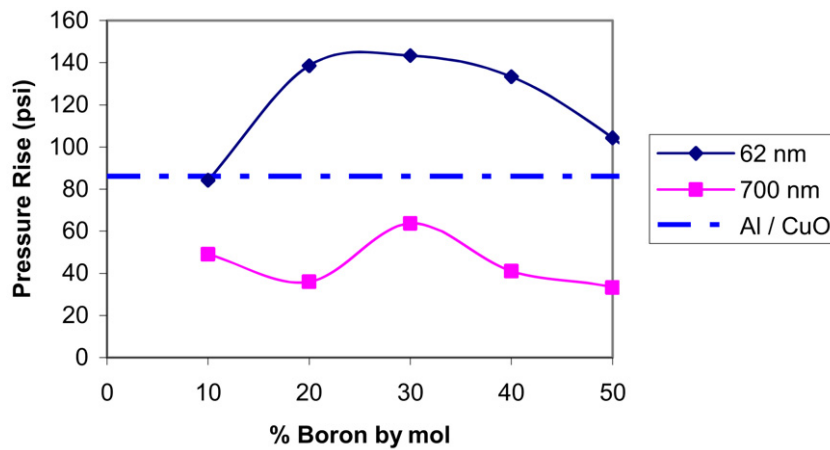
Fig. 5. Experimentally measured pressure rise in the region where an enhanced reactivity is observed (<50% B by mol).

Filippov and Rosner [31], and a polynomial fit is applied to write the Nusselt number as a function of temperature for the range of adiabatic flame temperatures achieved in the mixtures. This gives a range of Nusselt numbers from 0.06 to 0.13 for the 62 nm boron, and 0.34 to 0.54 for the 700 nm boron.

The thermal conductivity also changes as a function of the gas temperature and composition. The CHEETAH calculations (assuming B to be inert) were used to obtain the equilibrium species distribution. Since only nitrogen, oxygen and copper are in the product vapor an effective thermal conductivity is obtained as a molar average. For oxygen and nitrogen, the thermal conductivity as a function of temperature is given in Incropera and DeWitt [32] up to 3000 K, and we extrapolate it to 3500 K. For copper, the thermal conductivity can be estimated as a function of temperature using kinetic theory for a monatomic gas in terms of the atomic mass (m) and diameter (σ):

$$k(T) = \left(\frac{k_B T}{\pi^3 m \sigma^4} \right)^{1/2}. \tag{3}$$

The convection term has now been completely formulated as a function of temperature and particle properties. To calculate the total heating time, we calculate three individual processes.

(1) Sensible heating from room temperature to the surrounding temperature (Eq. (5)).
(2) Time to evaporate the initial B_2O_3 shell (constant $T_P = 2338$ K) (Eq. (6)).
(3) Time to melt the boron (constant $T_P = 2350$ K) (Eq. (7)). (Note: The time to melt the B_2O_3 shell is insignificant.)

We have included radiation heat loss by assuming the boron particles transfer energy to the pressure cell wall at 300 K (T_{Wall}). Here, ε is the emissivity of B_2O_3 (assumed to be 1), σ_B is the Stefan–Boltzmann constant, and A is the particle surface area,

$$\dot{q}_{Rad} = \varepsilon \sigma_B A \left(T_P^4 - T_{Wall}^4 \right). \tag{4}$$

The individual heating times for the above three cases can be obtained by integration of Eqs. (5)–(7), respectively:

$$\frac{dT_P}{dt} = \frac{(\dot{q}_{conv} - \dot{q}_{Rad})}{m C_P}, \tag{5}$$

$$\frac{dm}{dt} = \frac{(\dot{q}_{conv} - \dot{q}_{Rad})}{H_{Vap,B_2O_3}}, \tag{6}$$

$$\frac{dm}{dt} = \frac{(\dot{q}_{conv} - \dot{q}_{Rad})}{H_{Fus,B}}. \tag{7}$$

Here T_P is the particle temperature, m is the particle mass, C_P is the heat capacity, H_{Vap,B_2O_3} is the latent heat of vaporization

of B_2O_3 at 2338 K (5.19 MJ/kg), and $H_{Fus,B}$ is the latent heat of fusion for boron at 2350 K (4.64 MJ/kg). The heat capacity used was weighted (since both B and B_2O_3 are present in the particle), and was calculated as a function of particle temperature using the Shomate approximation of the coefficients in the NIST-JANAF thermochemical tables [33].

Equations (5)–(7) were numerically integrated, and the results of the model are shown for 62 nm boron and 700 nm boron in Figs. 6 and 7, respectively. The calculations indicate that the total time to heat the 62 nm boron up to the surrounding temperature is faster than 17 us, the Al/CuO time scale, at temperatures above 2370 K while for the 700 nm boron, the time always lags and does not become faster until the surrounding temperature is above 2800 K. It also is evident that the removal of the oxide shell alone cannot explain why 700 nm boron does not enhance the reactivity, since it is removed almost as quickly as in the case of 62 nm boron. However, we see that the sensible heating time for the micronboron is significantly longer than for the nanoboron, and we also see that the time required to melt the micron boron is over an order of magnitude longer than for the nanoboron. Thus, from the experimental and model results, it's reasonable to conclude that for boron to enhance the reactivity, the particles must be heated, have their oxide shell removed, and be melted on a timescale shorter than that for the thermite reaction in order to participate in the combustion and enhance the reactivity.

Boron's ability to enhance the reactivity is most likely due to the increased gas production when boron is present as a fuel. If the boron is able to participate in the combustion, it should oxidize to gaseous B_2O_3, along with sub-oxides such as BO and BO_2. As a result, the absolute pressure rise could be higher than that observed for Al/CuO, where the temperature is below the Al_2O_3 boiling point and thus the oxide product is molten. To investigate this, CHEETAH calculations were again performed, but now the boron was assumed to be reactive. The adiabatic temperature and gas species distribution as a function of % B are shown in Fig. 8, and the formation of a significant amount of boron oxide species (BO, BO_2, B_2O_3) in the products can be seen. The calculation predicts the total gas production to increase relative to an Al/CuO mixture, where copper is the only major gas product. The increase in gaseous products increases the total pressure, and this was consistent with the experimental data (Fig. 5).

Not only does gas production affect the pressure rise, it can also affect the rise time. This is because the mode of energy propagation through a loose powder MIC is speculated to be primarily via convection of gaseous intermediate species [34]. Other experimental works [28] show a correlation between the peak reactivity
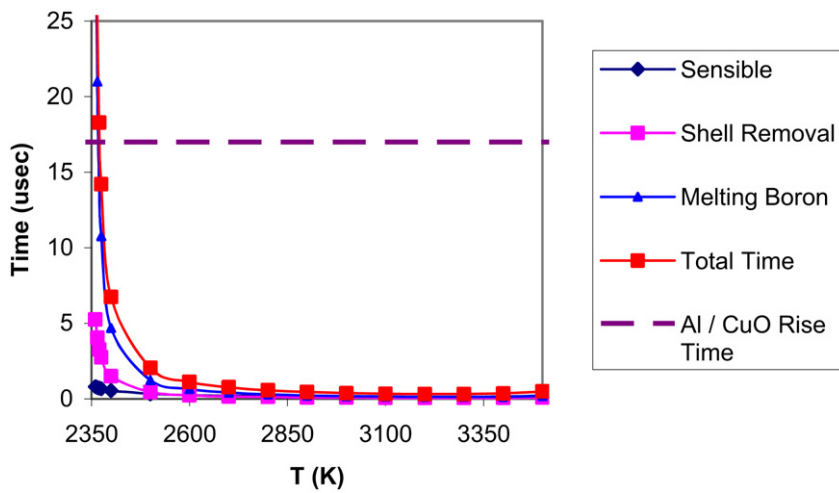
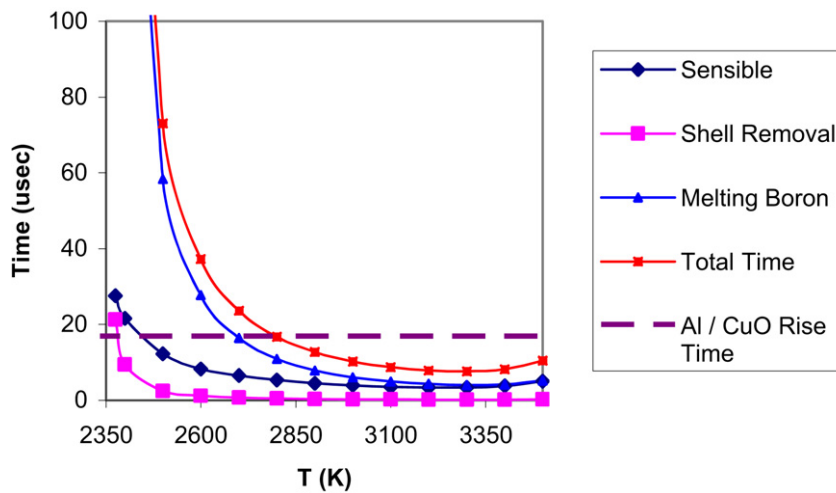**Fig. 6.** Model predictions of the timescales as a function of surrounding temperature for a 700 nm boron particle.

Fig. 7. Model predictions of the timescales as a function of surrounding temperature for a 700 nm boron particle.
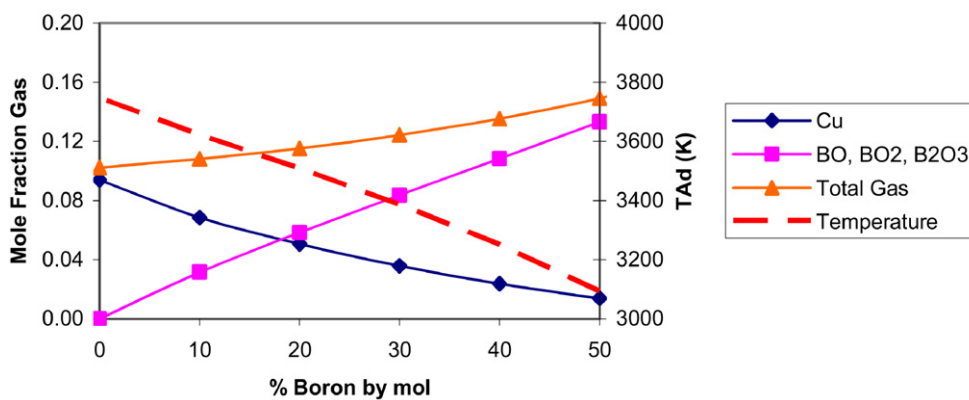

Fig. 8. Adiabatic temperature and equilibrium gas species composition assuming boron to be reactive.

and the peak gas production, but this does not necessarily correspond to the maximum temperature. In this work, the pressure rise time does become faster (see Fig. 4) for the cases where the enhancement was seen. This is likely a result of the increased gas production aiding in the convective energy propagation through the loose powder.

A major assumption in our model was that the convective heat transfer to the particle only happened through collisions with gaseous species. However, additionally there could be condensation of intermediate gaseous species, such as copper, onto the particles. This heat of condensation would enhance the heat transfer to the particles, and decrease the time to heat the boron even further than predicted by the model. However, a layer of condensed material on the particles would serve as a barrier to oxidation much like the B_2O_3 does if it is not removed. The complexities of that effect are beyond the scope of this investigation.

4. Conclusions

It has been demonstrated from constant-volume combustion studies that the addition of nanoboron to a MIC of Al/CuO can enhance the reactivity when the boron is <50 mol% of the fuel, while an enhancement was not observed when micronboron was used instead. Thermodynamic calculations assuming the boron to be inert showed that the aluminum reaction with CuO was able to raise the mixture temperature above 2350 K, above the boiling point of B_2O_3 and melting point of boron. This led to the development of a phenomenological heat transfer model which investigated the sensible and latent heating time for boron particles surrounded by a high-temperature environment. The model shows the heating time becomes faster than the Al/CuO reaction time, 17 us, at temperatures above 2370 K for the nanoboron and above 2800 K for the larger boron. The heating time for the micronboron severely lags because of the very large time to melt the boron. From the experimental and model results, we speculate that not only is the sensible heating and removal of the oxide shell necessary for fast reaction, the melting of the boron is also critical.

Acknowledgments

References

[1] T.A. Brzustowski, I. Glassman, 1964, IAA Accession No. A65-10970, 33 pp.
[2] I. Glassman, Metal Combustion Process, Preprint, American Rocket Society, New York, 1959.
[3] E.W. Price, Prog. Astronaut. Aeronaut. 90 (1983) 479–513.
[4] M.A. Trunov, M. Schoenitz, X. Zhu, E.L. Dreizin, Combust. Flame 140 (4) (2005) 310–318.
[5] A. Rai, K. Park, L. Zhou, M.R. Zachariah, Combust. Theory Modelling 10 (5) (2006) 843–859.
[6] S.E. Olsen, M.W. Beckstead, J. Propul. Power 12 (4) (1996) 662–671.
[7] A. Macek, J.M. Semple, Combust. Sci. Technol. 1 (3) (1969) 181–191.
[8] A. Ulas, K.K. Kuo, C. Gotzmer, Combust. Flame 127 (1/2) (2001) 1935–1957.
[9] I. Glassman, F.A. Williams, P. Antaki, in: The Combustion Institute, Pittsburgh, PA, 1984.
[10] M.K. King, in: CPIA Publication 529, 26th JANNAF Combustion Meeting, 1989.
[11] M.K. King, in: CPIA Publication 366, 19th JANNAF Combustion Meeting, 1982.
[12] M.K. King, Combust. Sci. Technol. 8 (5–6) (1974) 255–273.
[13] M.K. King, Combust. Sci. Technol. 5 (4) (1972) 155–164.
[14] C.L. Yeh, K.K. Kuo, Prog. Energy Combust. Sci. 22 (6) (1997) 511–541.
[15] I. Glassman, Combustion, third ed., Academic Press, San Diego, CA, 1996.
[16] R.A. Yetter, H. Rabitz, F.L. Dryer, R.C. Brown, C.E. Kolb, Combust. Flame 83 (1–2) (1991) 43–62.
[17] A. Macek, J.M. Semple, Proc. Combust. Inst. 13 (1971) 859–868.
[18] E.M. Hunt, M.L. Pantoya, J. Appl. Phys. 98 (3) (2005) 034909/1–034909/8.
[19] K. Park, D. Lee, A. Rai, D. Mukherjee, M.R. Zachariah, J. Phys. Chem. B 109 (15) (2005) 7290–7299.
[20] T. Parr, C. Johnson, D. Hanson-Parr, K. Higa, K. Wilson, in: JANNAF Combustion Subcommittee Meeting, December, 2003.
[21] T. Bazyn, H. Krier, N. Glumac, Combust. Flame 145 (4) (2006) 703–713.
[22] C.E. Aumann, G.L. Skofronick, J.A. Martin, J. Vac. Sci. Technol. B: Microelectron. Nanometer Struct. 13 (3) (1995) 1178–1183.
[23] J. Katz, F. Tepper, G.V. Ivanov, M.I. Lerner, V. Davidovich, in: CPIA Publication 675, JANNAF Propulsion Meeting, 1998.
[24] Y. Yang, S. Wang, Z. Sun, D.D. Dlott, Propell. Explos. Pyrotech. 30 (3) (2005) 171–177.
[25] S.F. Son, J.R. Busse, B.W. Asay, P.D. Peterson, J.T. Mang, B. Bockmon, M.L. Pantoya, Proc. Int. Pyrotech. Seminar 29 (2002) 203–212.
[26] B.S. Bockmon, M.L. Pantoya, S.F. Son, B.W. Asay, J.T. Mang, J. Appl. Phys. 98 (6) (2005) 064903/1–064903/7.
[27] J.Y. Malchi, R.A. Yetter, T.J. Foley, S.F. Son, Combust. Sci. Technol. 180 (7) (2008) 1278–1294.
[28] V.E. Sanders, B.W. Asay, T.J. Foley, B.C. Tappan, A.N. Pacheco, S.F. Son, J. Propul. Power 23 (4) (2007) 707–714.
[29] A. Prakash, A.V. McCormick, M.R. Zachariah, Adv. Mater. (Weinheim, Germany) 17 (7) (2005) 900–903.
[30] M.L. Hobbs, M.R. Baer, B.C. McGee, Propell. Explos. Pyrotech. 24 (5) (1999) 269–279.
[31] A.V. Filippov, D.E. Rosner, Int. J. Heat Mass Transfer 43 (1) (1999) 127–138.
[32] F.P. Incropera, D.P. DeWitt, Fundamentals of Heat and Mass Transfer, third ed., John Wiley and Sons, New York, 1990.
[33] M.W. Chase Jr., J. Phys. Chem. Ref. Data Monograph 9 (1998) 1–1951.
[34] B.W. Asay, S.F. Son, J.R. Busse, D.M. Oschwald, AIP Conference Proceedings, 706 (Pt. 2, Shock Compression of Condensed Matter–2003, Part 2), 2004, pp. 827–830.